Nanotheranostics: Congo Red/Rutin-MNPs with Enhanced Magnetic Resonance Imaging and H_2O_2-Responsive Therapy of Alzheimer's Disease in APPswe/PS1dE9 Transgenic Mice

Bingbing Hu, Fengying Dai, Zhanming Fan, Guanghui Ma, Qunwei Tang, and Xin Zhang**

Alzheimer's disease (AD) is the most common neurodegenerative disorder. The pathological hallmarks of AD are the extracellular accumulations of the senile plaques formed by amyloid beta (Aβ) aggregation and cerebral amyloid angiopathy as well as intracellular neurofibrillary tangles formed by hyperphosphorylated tau.[1] Although the molecular mechanisms of AD pathogenesis have not been clearly understood due to its complexity, recent advances have demonstrated that Aβ generates reactive oxygen species (ROS) such as hydrogen peroxide (H_2O_2) in the presence of metal ions, especially copper and zinc ions.[2] Increased ROS can facilitate Aβ plaques' production and accumulation, which can also induce nitric oxide (NO) generation, leading to neuronal death.[3] Thus, Aβ plaques' molecular imaging may be a useful method in the diagnosis of prodromal AD, and reducing Aβ-induced oxidative stress will be an attractive therapeutic and preventive strategy in the development of disease-modifying drugs for AD. It is therefore necessary to develop more efficient and safe theranostics systems of AD.

Theranostics systems of AD need to satisfy the following conditions: (1) there should be diagnostic probes that can image amyloid plaques in vivo and (2) theranostics systems should have the abilities of targeted delivery and controlled release of therapeutic agents. However, there is no such theranostics system of AD reported. Prior studies are focused on either the imaging of amyloid plaques or the delivery of drugs.[4a,b] Yang and co-workers have designed Aβ-peptide-loaded iron oxide nanoparticles to detect amyloid plaques in vivo by magnetic resonance imaging (MRI).[4c] Wilson and co-workers have used chitosan nanoparticles for the delivery of rivastigmine to treat AD, however these nanoparticles do not have the abilities of targeted delivery and controlled release of drugs.[4b] If the abilities of imaging amyloid plaques and targeted delivery and controlled release of drugs can be combined, theranostics systems of AD will be achieved.

Iron oxide nanoparticles, which have high relaxivity for MRI, a long half-life, and can be covalently conjugated to drugs and antibodies, may emerge as a new paradigm for nanotheranostics applications for AD.[5] Since AD is accompanied by neuroinflammation, which compromises the blood–brain barrier (BBB),[6] ultrasmall superparamagnetic iron oxide nanoparticles (USPIONs) can penetrate the BBB to some extent;[7] and for the imaging of amyloid plaques by MRI and targeted delivery of drugs, some molecules that can bind to amyloid plaques, such as Aβ peptides, anti-Aβ antibody, and Congo red, can be used to label USPIONs.[4c,8] The design of nanosystems with stimuli-responsiveness properties, according to the physiological differences between lesions and normal tissues, will open new avenues for the development of intelligent biomedical platforms with controlled drug release properties.[9] Qu and co-workers have designed mesoporous silica nanoparticles and gold nanocages as drug delivery carriers, and have used IgG as caps. The opening protocol and delivery of the entrapped drugs depended on the presence of the H_2O_2 to which the arylboronic esters are expected to be oxidized to phenols. The complete breakage of the arylboronic esters should result in the release of IgG and subsequently the drugs.[2b,c] In view of the fact that Aβ aggregation generates ROS such as H_2O_2 in the presence of metal ions, targeting molecules-loaded USPIONs can be designed as theranostics nanosystems with H_2O_2-responsiveness, which combine the abilities of detecting amyloid plaques by MRI and targeted delivery and controlled release of drugs.

Considering that Congo red can specifically detect amyloid plaques[10] and arylboronic ester is redox sensitive,[2b,c,d,11] we report the biocompatible nanotheranostics system based on iron oxide magnetic nanoparticles with ultrasmall size and excellent magnetic property to realize MRI of amyloid plaques and targeted delivery and H_2O_2 controlled release of AD therapeutic agents. The advantages of this system can be listed as

B. Hu, Prof. G. Ma, Prof. X. Zhang
National Key Laboratory of Biochemical Engineering
Institute of Process Engineering
Chinese Academy of Sciences
Beijing 100190, P. R. China
E-mail: xzhang@ipe.ac.cn
B. Hu, Prof. Q. Tang
Institute of Materials Science and Engineering
Ocean University of China
Qingdao 266100, P. R. China
E-mail: tangqunwei@ouc.edu.cn
Dr. F. Dai
Beijing Center for Physical and Chemical Analysis
Beijing 100084, P. R. China
Prof. Z. Fan
Department of Radioloy
Beijing Anzhen Hospital
Capital University
Beijing 100029, P. R. China

DOI: 10.1002/adma.201502227

follows: (1) as Congo red has the ability to bind to amyloid plaques that have extensive β-sheet structures, Congo red loaded magnetic nanoparticles can specifically bind to amyloid plaques and give a greater contrast-to-noise ratio on MRI; (2) the release of drugs can be triggered by H_2O_2, caused by deviant Aβ-metal interactions in AD due to the H_2O_2-responsiveness of the boronate ester bond between the vicinal diols of the therapeutic agent Rutin and phenylboronic acid; (3) Rutin is a glycone of quercetin with a flavonol structure and is a powerful phenolic antioxidant that has various pharmacological properties, including antitumor, anti-inflammatory, antidiarrheal, antimutagenic, myocardial protecting, and immunemodulator. Wang and co-workers have demonstrated that Rutin could interfere with Aβ aggregation and neurotoxicity, prevent oxidative stress induced by Aβ, reduce Aβ levels in mutant neurons, and decrease senile plaques in the brains of AD transgenic mice.[12]

In this system, to obtain ultrasmall magnetic nanoparticles, we synthesised oleic acid coated iron oxide nanoparticles by the thermal decomposition method. 1,2-dioleoyl-*sn*-glycero-3-phosphoethanolamine-*n*-[poly(ethylene glycol)]-Congo red (DSPE-PEG-Congo red) and 1,2-dioleoyl-*sn*-glycero-3-phosphoethanolamine-*n*-[poly(ethylene glycol)]-phenylboronic acid (DSPE-PEG-phenylboronic acid) were prepared by conjugating 1,2-dioleoyl-*sn*-glycero-3-phosphoethanolamine-*n*-[poly(ethylene glycol)]-hydroxy succinamide (DSPE-PEG-NHS) with Congo red and 3-aminophenylboronic acid (Figure S1, Supporting Information).[13] As illustrated in **Figure 1**A, DSPE-PEG-Congo red and DSPE-PEG-phenylboronic acid were used to improve the biocompatibility of oleic acid coated iron oxide nanoparticles through a micelle formation procedure.[14] The attachment of PEG onto the surface of magnetic nanoparticles had been shown to inhibit its uptake by the reticuloendothelial system and prolong circulation, thus promoting delivery to the central nervous system. At the same time, PEG would improve the contrast efficiency by enhancing water diffusion in close proximity to the nanocrystal core, provide appropriate biocompatibility, improve colloidal stability, and retain desired magnetic properties such as high r_2 values for MRI.[5a,15] The hydrophilic drug Rutin was then grafted onto the surface of the nanoparticles through the formation of boronate ester bond between vicinal diols and phenylboronic acid.[2c,d,16] As shown in Figure 1B, (1) Congo red/Rutin-MNPs coinjected with mannitol could penetrate the BBB into the brain of the APPswe/PS1dE9 transgenic mouse and bind to amyloid plaques, which allowed the detection of amyloid plaques by MRI and achieved a targeted delivery of drugs; (2) The Aβ-induced production of H_2O_2 could oxidize arylboronic esters to phenols, resulting in the release of Rutin that would prevent oxidative stress and reduce amyloid plaques and neuronal loss.

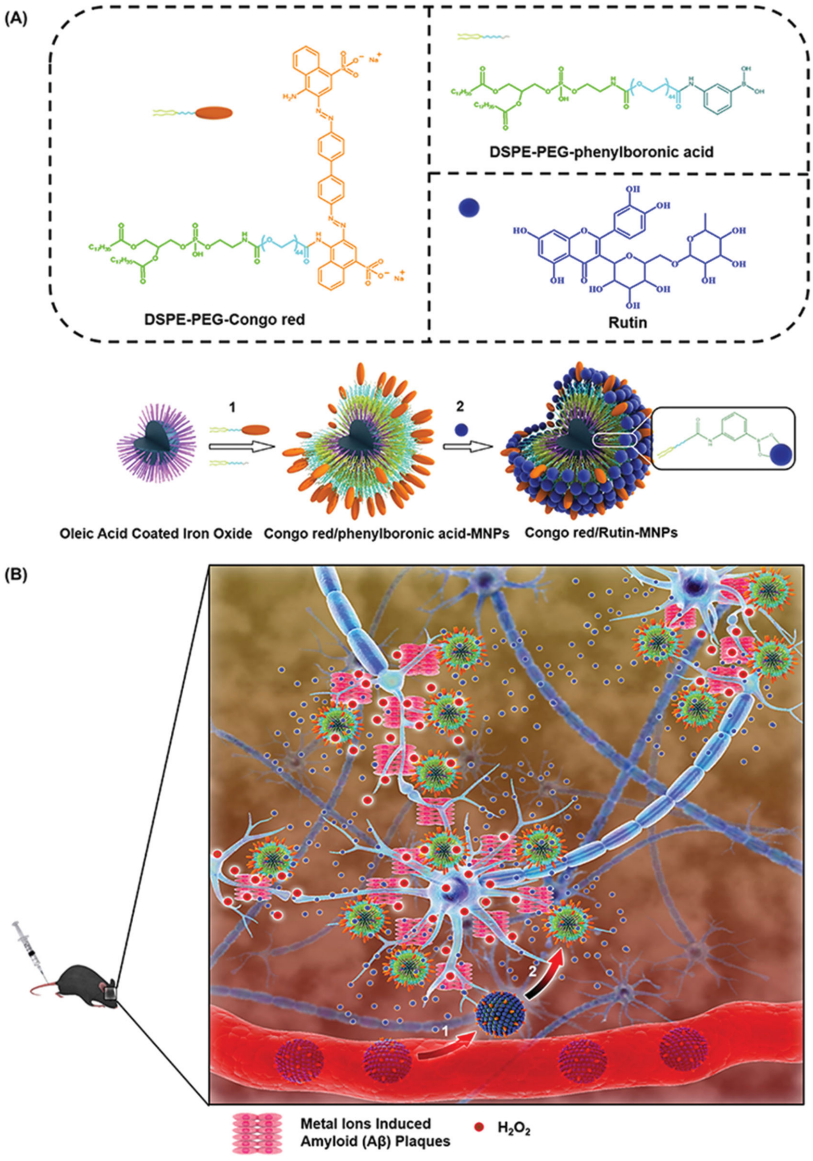

Figure 1. A) The preparation of Congo red and Rutin loaded magnetic nanoparticles (Congo red/Rutin-MNPs): (1) DSPE-PEG-Congo red and DSPE-PEG-phenylboronic acid were used to improve the biocompatibility of magnetic nanoparticles through a micelle formation procedure. (2) Rutin was grafted onto the surface of the nanoparticles through the formation of a boronate ester bond between vicinal diols and phenylboronic acid. B) Schematic interpretation of Congo red/Rutin-MNPs in vivo: (1) Congo red/Rutin-MNPs co-injected with mannitol penetrated the BBB. (2) Congo red/Rutin-MNPs detected amyloid plaques specifically, realized targeted delivery and controlled release of Rutin by H_2O_2.

The chemical composition of the obtained polymers was studied by ^{1}H NMR spectra (Figure S2, Supporting Information), which suggested the successful synthesis of DSPE-PEG-Congo red and DSPE-PEG-phenylboronic acid. We obtained a series of magnetic nanoparticles with different amounts of

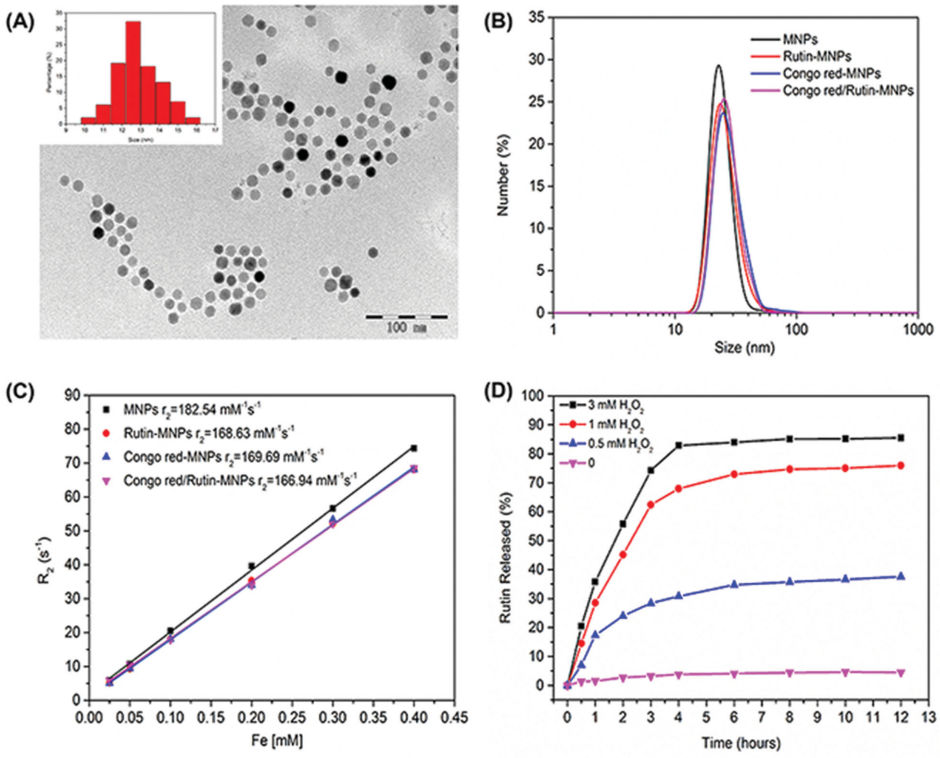

Figure 2. Characterization of magnetic nanoparticles. A) The TEM image of Congo red/Rutin-MNPs (inset: the size distribution histograms of nanoparticles, a total of 110 nanoparticles were counted). The scale bar corresponds to 100 nm. B) The hydrodynamic sizes of MNPs, Rutin-MNPs, Congo red-MNPs, and Congo red/Rutin-MNPs. C) The r_2 values of MNPs, Rutin-MNPs, Congo red-MNPs, and Congo red/Rutin-MNPs. D) Release profiles of Rutin from Congo red/Rutin-MNPs triggered by different concentrations of H_2O_2.

Congo red and Rutin by changing the amounts of DSPE-PEG-Congo red and DSPE-PEG-phenylboronic acid. As the absorptions of Rutin are around 250–350 nm and Congo red around 350–500 nm, loadings of Congo red and Rutin were measured by UV–vis spectra (Figure S3, Supporting Information). Transmission electron microscope (TEM) images of magnetic nanoparticles presented monodispersed and spherical-like structures with the diameter of about 13 nm (**Figure 2**A). As shown in Figure 2B, the hydrodynamic sizes of nanoparticles were about the same, which showed that the modification of DSPE-PEG coated iron oxide nanoparticles did not change their dispersity. In addition, the zeta potentials of nanoparticles were close to electric neutrality and the results of serum stability showed that the nanoparticles were stable without aggregation in serum, which indicated that the nanoparticles would have biocompatibility and stability in vivo (Figure S4, Supporting Information). To further assess their magnetic properties for MRI application, r_2 values of the nanoparticles were calculated by measuring the change in the spin–spin relaxation rate (R_2) per unit iron concentration. The r_2 value of MNPs (DSPE-PEG coated magnetic nanoparticles) was a little higher than that of the Congo red/Rutin-MNPs, indicating that the conjugation of Congo red and Rutin had little impact on the r_2 value of the nanoparticles as shown in Figure 2C. These results demonstrated that the Congo red/Rutin-MNPs had excellent r_2 values and motivated us to examine the application of the magnetic nanoparticles as a novel contrast agent for in vivo MRI of AD. The release experiments were performed in PBS (0.01 M, pH 7.4) with different concentrations of H_2O_2, as it was previously reported that cells had H_2O_2 concentrations of up to 1×10^{-3} M.[2b,c] The release of the Rutin depended on the degradation of boronate ester bonds by H_2O_2. Figure 2D shows that the amounts of Rutin released reached about 85%, 75%, and 35% after 12 h of incubation upon 3×10^{-3}, 1×10^{-3}, and 0.5×10^{-3} M H_2O_2, whereas only 4% release was obtained without H_2O_2. The result indicated that the release of Rutin was H_2O_2-responsive and concentration dependent.

Before in vivo imaging and therapy, we tested the feasibility of Congo red/Rutin-MNPs for AD therapeutic applications in vitro studies. Metal ions such as copper and zinc ions could induce Aβ aggregation and form neurotoxic ROS (e.g. H_2O_2). So, the effects of Congo red/Rutin-MNPs on Aβ aggregation-induced cytotoxicity using SH-SY5Y neuroblastoma cells were studied by the methylthiazolyltetrazolium method.[4a,12a] All assays were conducted under the same conditions and data were normalized using the results from cells not treated with Aβ+Cu^{2+}, which acted as a positive control. As shown in **Figure 3**A, the treatment of cells with Aβ+Cu^{2+} reduced the cell viability to 67%, and the addition of Congo red, MNPs, and Congo red-MNPs could not reduce the Aβ-induced cytotoxicity. Due to the neuroprotective effects of Rutin, the survival of the cells increased to about 92% in the presence of Rutin. Moreover, as a result of Rutin, treatment of cells with Rutin-MNPs that had no targeted molecular Congo red reduced cytotoxicity

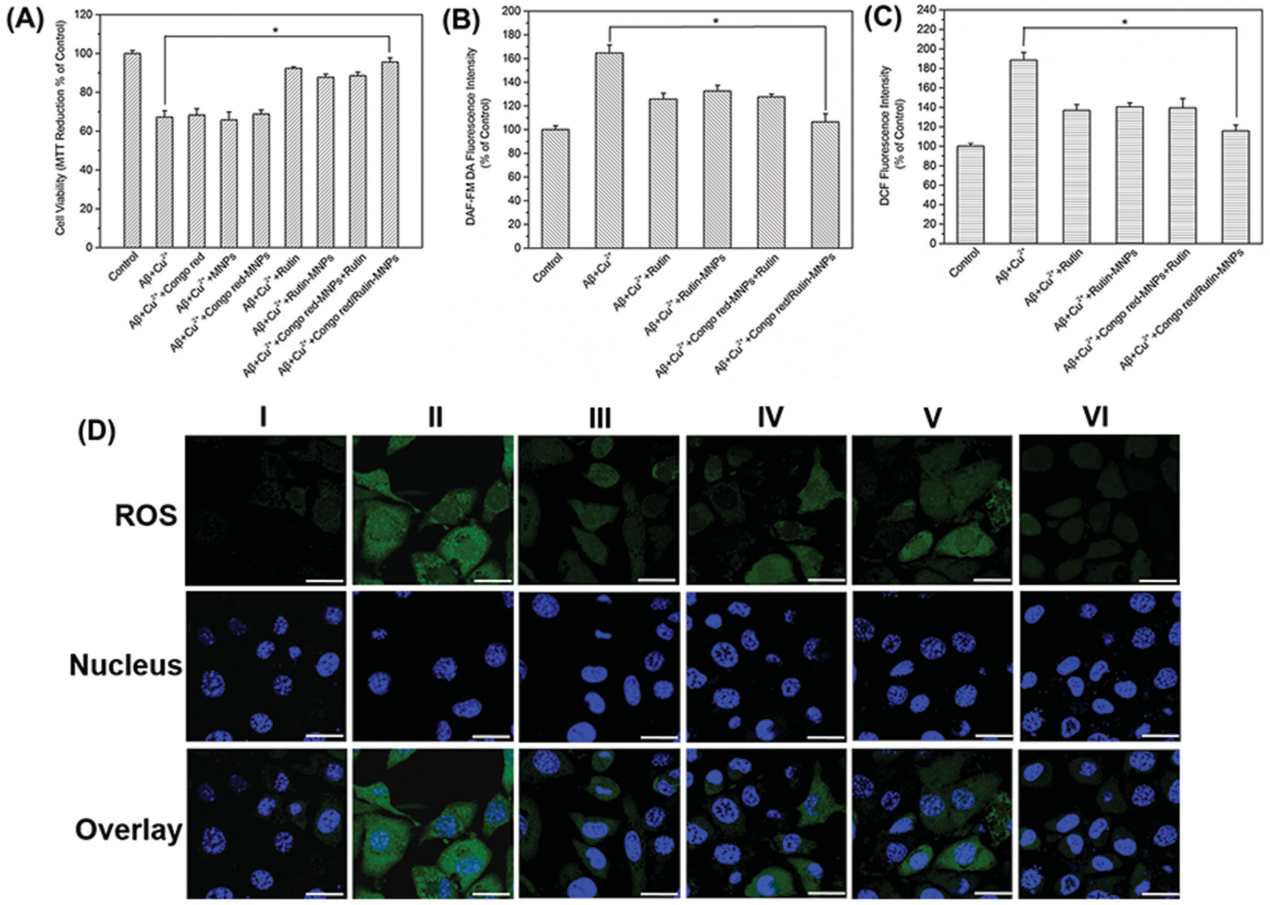

Figure 3. In vitro cell studies. A) Protection effects of Congo red/Rutin-MNPs on Aβ-induced cytotoxicity of SH-SY5Y cells. B) The effect of Congo red/Rutin-MNPs on production of NO. C) The effect of Congo red/Rutin-MNPs on Aβ-induced production of ROS. D) Confocal microscopic images of cells ROS. The scale bars correspond to 25 μm. ((I) control, (II) Aβ+Cu^{2+}, (III) Aβ+Cu^{2+}+Rutin, (IV) Aβ+Cu^{2+}+Rutin-MNPs, (V) Aβ+Cu^{2+}+Congo red-MNPs+Rutin, (VI) Aβ+Cu^{2+}+Congo red/Rutin-MNPs) Control: Aβ+Cu^{2+}-untreated cells, [Aβ42] = 10×10^{-6} M, [Cu^{2+}] = 10×10^{-6} M, [Congo red] = 0.1 mg mL^{-1}, [Rutin] = 0.1 mg mL^{-1}, [MNPs] = 1 mg mL^{-1}, [Congo red/Rutin-MNPs] = 1 mg mL^{-1}, [Rutin-MNPs] = 1 mg mL^{-1}, [Congo red-MNPs] = 1 mg mL^{-1} ($^*P < 0.05$).

and Congo red-MNPs+Rutin also increased the cell viability to about 90%. As expected, the cell viability also increased to about 95% in the presence of Congo red/Rutin-MNPs, which indicated that our delivery system had better protective effects on Aβ-induced cytotoxicity of SH-SY5Y cells.

NO plays a pivotal role in the cascade of events leading to neuronal death, and the Aβ aggregation can induce NO generation by upregulating the expressing of NO synthase. To investigate the effect of Congo red/Rutin-MNPs against NO, 3-amino,4-aminomethyl-2′,7′-difluorofluorescein diacetate (DAF-FM DA) was used as a probe for NO.[17] As shown in Figure 3B, exposure of cells to Aβ+Cu^{2+} increased the content of NO to about 165% relative to untreated control cells. And Congo red, MNPs, and Congo red-MNPs had no effect on reducing the production of NO (Figure S6A, Supporting Information). In the presence of Rutin, the levels of NO decreased to about 125%. In addition, the treatment of cells with Rutin-MNPs or Congo red-MNPs+Rutin caused the levels of NO to diminish by 30% and 34%, respectively, compared to cells exposed only to Aβ+Cu^{2+}. Importantly, the level of NO also decreased to about 105% in the presence of Congo red/Rutin-MNPs, which showed that the Congo red/Rutin-MNPs effectively reduced the generation of NO.

The formation of ROS by Aβ+Cu^{2+} has been suggested as a proposed mechanism of AD pathogenesis. ROS can cause oxidative stress that would trigger a series of damages to cellular components. The success in the inhibition of Aβ-induced cytotoxicity and decreasing NO promoted us to examine the effect of Congo red/Rutin-MNPs against ROS. We used 2′,7′-dichlorodihydrofluorescein diacetate (DCFH-DA) as a probe for ROS because it could become fluorescent DCF via oxidation by ROS.[18] The changes in ROS were monitored by confocal microscopic images (Figure 3D) and quantification was further given in Figure 3C. In the presence of Aβ+Cu^{2+}, the level of ROS was increased to about 188% relative to the control cells, while Congo red, MNPs, and Congo red-MNPs had no effect on Aβ-induced production of ROS (Figure S6B, Supporting Information). The treatment of cells with Rutin reduced the ROS level to about 135%. Furthermore, the treatment of cells with Rutin-MNPs or Congo red-MNPs+Rutin diminished the levels of ROS by 48% and 50%, respectively, compared to cells

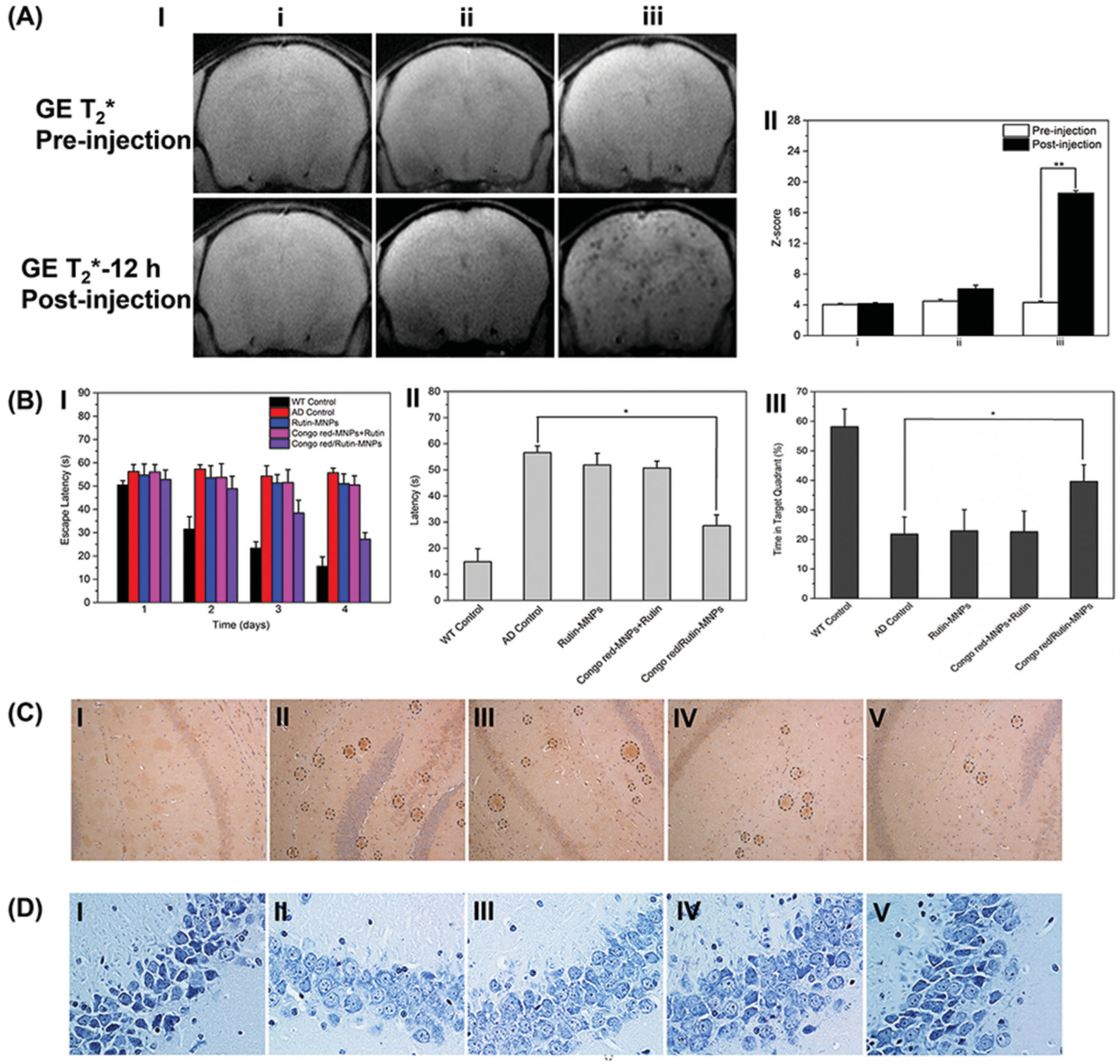

Figure 4. In vivo experiments. A) (I) Representative in vivo 7 Tesla MR images of brains in WT mice before and 12 h after intravenous injection of Congo red/Rutin-MNPs (i), AD mice before and 12 h after intravenous injection of Rutin-MNPs (ii), and Congo red/Rutin-MNPs (iii). (II) Z-scores from the MRI data among WT mice before and 12 h after intravenous injection of Congo red/Rutin-MNPs, AD mice before and 12 h after intravenous injection of Rutin-MNPs and Congo red/Rutin-MNPs. B) (I) The escape latencies of WT control mice, AD control mice, and AD mice treated with Rutin-MNPs, Congo red-MNPs+Rutin, and Congo red/Rutin-MNPs. (II) The latency during the memory test in the MWM probe trial without a platform. (III) The percent (%) of time in the targeted quadrant where the platform had been located during the memory test in the MWM probe trial. C) The immunohistochemical analysis of Aβ deposition in the brains of WT control mice (I), AD control mice (II), AD mice treated with Rutin-MNPs (III), Congo red-MNPs+Rutin (IV), and Congo red/Rutin-MNPs (V). The Aβ depositions were brown signals as indicated by black dotted circle. D) The Nissl staining of nerve cells in the brains of WT control mice (I), AD control mice (II), AD mice treated with Rutin-MNPs (III), Congo red-MNPs+Rutin (IV), and Congo red/Rutin-MNPs (V). The Nissl bodies were stained blue ($^*P < 0.05$, $^{**}P < 0.01$).

exposed to Aβ+Cu^{2+}. As expected, treating the cells with Congo red/Rutin-MNPs caused a marked reduction in the ROS level. Therefore, in vitro studies showed the feasibility of the Congo red/Rutin-MNPs system for AD therapeutic applications.

In order to test the ability of Congo red loaded magnetic nanoparticles to detect amyloid plaques specifically, UV–vis spectra of Congo red and Congo red/Rutin-MNPs in the presence of FBS and Aβ42 were measured. As Congo red had the ability to bind to amyloid plaques that have extensive β-sheet structures, the UV–vis spectra should have a redshift.[10] The result showed that there were only redshifts in the spectra of Congo red and Congo red/Rutin-MNPs in the presence of Aβ42 (Figure S5A, Supporting Information). In addition, the Prussian-blue staining of SH-SY5Y neuroblastoma cells showed

that many nanoparticles could be stained only in the presence of both Congo red/Rutin-MNPs and Aβ42 (Figure S5 B, Supporting Information). These results indicated that Congo red/Rutin-MNPs could target amyloid plaques specifically in vitro. Moreover, a 7 Tesla MRI scanner was used for imaging wild type mice (WT mice) treated with Congo red/Rutin-MNPs and APPswe/PS1dE9 transgenic mice (AD mice) treated with Congo red/Rutin-MNPs and Rutin-MNPs. As shown in **Figure 4**A (I), 12 h after the intravenous injection of Congo red/Rutin-MNPs resulted in the detection of numerous dark spots in AD mice brains using in vivo T_2*-weight MRI and the analysis of colocalization immunohistochemistry also showed the presence of plaques on the same locations of the same layers from the same mouse (Figure S7, Supporting Information). There were almost no plaques detected in the brains of WT mice treated with Congo red/Rutin-MNPs and AD mice treated with Rutin-MNPs. In order to quantitatively assess the contrast enhancement capability, the MRI slices were analysed by calculating the contrast-to-noise ratio commonly called the *Z*-score, which is the number of standard deviations the MRI signal decreased by in the core of the plaque, versus the background noise in the image of the surrounding tissue.[8b,10d] The MRI and changes in *Z*-scores after the injection of Congo red/Rutin-MNPs indicated that Congo red/Rutin-MNPs would generally bind to amyloid plaques 6–12 h after injection (Figure S8, Supporting Information). *Z*-scores increased distinctly 12 h after injection of Congo red/Rutin-MNPs, which was about four times higher than that of preinjection, while there was no significant change in terms of the *Z*-scores in AD mice treated with Rutin-MNPs or WT mice treated with Congo red/Rutin-MNPs (Figure 4A (II)). These results indicated that Congo red-loaded magnetic nanoparticles could specifically bind to amyloid plaques and give a greater contrast-to-noise ratio on MRI. In addition, to better understand biodistribution and elimination of the nanoparticles, major organs including brain, heart, liver, spleen, lung, and kidney were harvested and stained by Prussian blue before and 12 h, 60 h after injection of Congo red/Rutin-MNPs (Figure S9, Supporting Information). The results showed that nanoparticles could accumulate in the brain. A small amount of nanoparticle accumulation was found in liver and spleen, which might be attributed to the macrophages endocytosis of nanoparticles by reticuloendothelial systems. 60 h after injection, there was almost no nanoparticle in brain and other organs, which indicated that Congo red/Rutin-MNPs were metabolized from the body. According to previous studies, the iron oxide nanoparticles were metabolized and the iron contained in Congo red/Rutin-MNPs was incorporated into the body's iron store as ferritin.[19]

The effect of Congo red/Rutin-MNPs on the spatial cognitive performance of APPswe/PS1dE9 transgenic mice was investigated through the Morris water maze (MWM) test.[1b,4b,12b] Escape latencies to find the hidden platform were measured daily (Figure 4B (I)). Both WT control mice and Congo red/Rutin-MNPs treated AD mice exhibited significantly shorter latency than AD control group on days 2, 3, and 4, indicating that Congo red/Rutin-MNPs could markedly improve the spatial memory of AD mice. After the last training, the platform was removed, and the mice were given 60 seconds to find the missing platform for the probe trial. As shown in Figure 4B (II), the Congo red/Rutin-MNPs treated AD mice exhibited spatially oriented swimming behavior and shorter latencies than AD control mice, Rutin-MNPs treated AD mice, and Congo red-MNPs+Rutin treated AD mice. Moreover, these outcomes were further confirmed by the percentage of time spent in the target quadrant (Figure 4B (III)). Overall, our results showed that Congo red/Rutin-MNPs could significantly rescue memory deficits in AD transgenic mice.

In order to further test the effects of Congo red/Rutin-MNPs on reducing amyloid plaques and inhibition of neuronal loss in the brains of AD mice, immunohistochemistry analysis and Nissl staining were performed to stain Aβ deposition and nerve cells in the brains. As shown in Figure 4C, a gross Aβ deposition difference was observed between the WT control mice and AD control mice. The Aβ plaque loads were not markedly decreased in the Rutin-MNPs and Congo red-MNPs+Rutin treated mice compared with the AD control mice. Nevertheless, there was a significant decrease in Aβ plaque loads in the brains of mice treated with Congo red/Rutin-MNPs, indicating that Congo red/Rutin-MNPs had the ability to reduce Aβ depositions. Furthermore, Figure 4D shows that neuronal hypocellularity was observed in the brains of the AD mice, which had very few Nissl bodies (blue). In contrast, Congo red/Rutin-MNPs treatment obviously attenuated neuron loss in AD control mice, whereas Rutin-MNPs and Congo red-MNPs+Rutin treatment had no significant effect. Compared with the results of the cell experiments, there were significant differences between Rutin-MNPs and Congo red/Rutin-MNPs in animal experiments. As Rutin-MNPs had no targeted molecules and Rutin in Congo red-MNPs+Rutin was a free drug, Rutin-MNPs and Congo red-MNPs+Rutin could not target to lesions and work effectively in vivo. Therefore, these results showed that Congo red/Rutin-MNPs had excellent therapeutic effects on AD.

In summary, we successfully developed Congo red/Rutin-MNPs nanotheranostics, which could specifically detect amyloid plaques by MRI, realize targeted delivery of AD therapeutic agents, achieve drug controlled release by H_2O_2 response, and prevent oxidative stress. Both in vitro and in vivo experiments were performed to justify this possibility and the remarkable disease-modifying effects of the nanotheranostics. It was found that Congo red/Rutin-MNPs could inhibit the Aβ-induced cytotoxicity and reduce the production of NO and ROS in vitro. More importantly, we found that following intravenous administration of Congo red/Rutin-MNPs resulted in detecting numerous amyloid plaques, rescuing memory deficits and ameliorating neurologic changes in APPswe/PS1dE9 transgenic mice brains. As nanotheranostics, Congo red/Rutin-MNPs would have clinical practicality, and could provide more efficient and safe theranostics systems of AD. If the costs could be further reduced, there would be more popular applications. In conclusion, our firstly reported Congo red/Rutin-MNPs nanotheranostics has the potential to open up a new avenue for AD theranostics applications.

Supporting Information

Supporting Information is available from the Wiley Online Library or from the author.

Acknowledgements

B.H. and F.D. contributed equally to this work. This work was financially supported by the National Natural Science Foundation of China (21304099, 51203162, 51373177), the National High Technology Research and Development Program (2014AA020708, 2012AA022703, 2012AA020804), the Instrument Developing Project of the Chinese Academy of Sciences (YZ201253, YZ201313), the Open Funding Project of the National Key Laboratory of Biochemical Engineering (Y22504A169), the "Strategic Priority Research Program" of the Chinese Academy of Sciences (XDA09030301-3), and Beijing Natural Science Foundation (Grant No. Z141100000214010). All procedures involving experimental animals were performed in accordance with protocols approved by the Institutional Animals Care and Use Committee of Peking University.

Received: May 9, 2015
Revised: July 8, 2015
Published online: August 13, 2015

[1] a) B. Dubois, H. H. Feldman, C. Jacova, H. Hampel, J. L. Molinuevo, K. Blennow, S. T. DeKosky, S. Gauthier, D. Selkoe, R. Bateman, S. Cappa, S. Crutch, S. Engelborghs, G. B. Frisoni, N. C. Fox, D. Galasko, M.-O. Habert, G. A. Jicha, A. Nordberg, F. Pasquier, G. Rabinovici, P. Robert, C. Rowe, S. Salloway, M. Sarazin, S. Epelbaum, L. C. de Souza, B. Vellas, P. J. Visser, L. Schneider, Y. Stern, P. Scheltens, J. L. Cummings, *Lancet Neurol.* **2014**, *13*, 614; b) Q. Song, M. Huang, L. Yao, X. Wang, X. Gu, J. Chen, J. Chen, J. Huang, Q. Hu, T. Kang, *ACS Nano* **2014**, *8*, 2345.

[2] a) G. Eskici, P. H. Axelsen, *Biochemistry* **2012**, *51*, 6289; b) J. Geng, M. Li, L. Wu, C. Chen, X. Qu, *Adv. Healthcare Mater.* **2012**, *1*, 332; c) P. Shi, M. Li, J. Ren, X. Qu, *Adv. Funct. Mater.* **2013**, *23*, 5412; d) Y. Wei, Y. Zhang, Z. Liu, M. Guo, *Chem. Commun.* **2010**, *46*, 4472.

[3] a) M. Rosini, E. Simoni, A. Milelli, A. Minarini, C. Melchiorre, *J. Med. Chem.* **2014**, *57*, 2821; b) H. P. Indo, H. C. Yen, I. Nakanishi, K. Matsumoto, M. Tamura, Y. Nagano, H. Matsui, O. Gusev, R. Cornette, T. Okuda, Y. Minamiyama, H. Ichikawa, S. Suenaga, M. Oki, T. Sato, T. Ozawa, D. K. St Clair, H. J. Majima, *J. Clin. Biochem. Nutr.* **2015**, *56*, 1.

[4] a) K. K. Cheng, P. S. Chan, S. Fan, S. M. Kwan, K. L. Yeung, Y. X. Wang, A. H. Chow, E. X. Wu, L. Baum, *Biomaterials* **2015**, *44*, 155; b) Z. Liu, M. Jiang, T. Kang, D. Miao, G. Gu, Q. Song, L. Yao, Q. Hu, Y. Tu, Z. Pang, H. Chen, X. Jiang, X. Gao, J. Chen, *Biomaterials* **2013**, *34*, 3870; c) J. Yang, Y. Z. Wadghiri, D. M. Hoang, W. Tsui, Y. Sun, E. Chung, Y. Li, A. Wang, M. de Leon, T. Wisniewski, *NeuroImage* **2011**, *55*, 1600; d) B. Wilson, M. K. Samanta, M. S. Muthu, G. Vinothapooshan, *Therapeutic. Delivery* **2011**, *2*, 599.

[5] a) J. F. Zeng, L. H. Jing, Y. Hou, M. X. Jiao, R. R. Qiao, Q. J. Jia, C. Y. Liu, F. Fang, H. Lei, M. Y. Gao, *Adv. Mater.* **2014**, *26*, 2694; b) H. B. Na, I. C. Song, T. Hyeon, *Adv. Mater.* **2009**, *21*, 2133; c) J. Qin, S. Laurent, Y. S. Jo, A. Roch, M. Mikhaylova, Z. M. Bhujwalla, R. N. Muller, M. Muhammed, *Adv. Mater.* **2007**, *19*, 1874; d) Y. Wang, H. C. Gu, *Adv. Mater.* **2015**, *27*, 576; e) M. Liong, C. Tassa, S. Y. Shaw, H. Lee, R. Weissleder, *Adv. Mater.* **2011**, *23*, H254; f) Y. Zhong, F. Dai, H. Deng, M. Du, X. Zhang, Q. Liu, X. Zhang, *J. Mater. Chem. B.* **2014**, *2*, 2938.

[6] a) V. C. Anderson, D. P. Lenar, J. F. Quinn, W. D. Rooney, *Cardiovasc. Psychiatry Neurol.* **2011**, *2011*, 615829; b) G. Bowman, J. Kaye, M. Moore, D. Waichunas, N. Carlson, J. Quinn, *Neurology* **2007**, *68*, 1809; c) B. Obermeier, R. Daneman, R. M. Ransohoff, *Nat. Med.* **2013**, *19*, 1584.

[7] J. S. Weinstein, C. G. Varallyay, E. Dosa, S. Gahramanov, B. Hamilton, W. D. Rooney, L. L. Muldoon, E. A. Neuwelt, *J. Cereb. Blood Flow Metab.* **2010**, *30*, 15.

[8] a) Y. Z. Wadghiri, J. Li, J. Wang, D. M. Hoang, Y. Sun, H. Xu, W. Tsui, Y. Li, A. Boutajangout, A. Wang, M. de Leon, T. Wisniewski, *PloS One* **2013**, *8*, e57097; b) L. O. Sillerud, N. O. Solberg, R. Chamberlain, R. A. Orlando, J. E. Heidrich, D. C. Brown, C. I. Brady, T. A. Vander Jagt, M. Garwood, D. L. Vander Jagt, *J. Alzheimers. Dis.* **2013**, *34*, 349; c) K. L. Viola, J. Sbarboro, R. Sureka, M. De, M. A. Bicca, J. Wang, S. Vasavada, S. Satpathy, S. Wu, H. Joshi, P. T. Velasco, K. MacRenaris, E. A. Waters, C. Lu, J. Phan, P. Lacor, P. Prasad, V. P. Dravid, W. L. Klein, *Nat. Nanotechnol.* **2015**, *10*, 91; d) J. H. Kim, T. L. Ha, G. H. Im, J. Yang, S. W. Seo, I. S. Lee, J. H. Lee, *Neuroreport* **2013**, *24*, 16; e) S. Li, H. He, W. Cui, B. Gu, J. Li, Z. Qi, G. Zhou, C. M. Liang, X. Y. Feng, *Anat. Rec.* **2010**, *293*, 2136.

[9] a) M. Wu, Q. Meng, Y. Chen, P. Xu, S. Zhang, Y. Li, L. Zhang, M. Wang, H. Yao, J. Shi, *Adv. Funct. Mater.* **2014**, *24*, 4273; b) B. P. Timko, T. Dvir, D. S. Kohane, *Adv. Mater.* **2010**, *22*, 4925.

[10] a) T. T. Ashburn, H. Han, B. F. McGuinness, P. T. Lansbury, *Chem. Biol.* **1996**, *3*, 351; b) W. E. Klunk, B. J. Bacskai, C. A. Mathis, S. T. Kajdasz, M. E. McLellan, M. P. Frosch, M. L. Debnath, D. P. Holt, Y. Wang, B. T. Hyman, *J. Neuropathol. Exp. Neurol.* **2002**, *61*, 797; c) C. Lendel, B. Bolognesi, A. Wahlstrom, C. M. Dobson, A. Graslund, *Biochemistry* **2010**, *49*, 1358; d) N. O. Solberg, R. Chamberlin, J. R. Vigil, L. M. Deck, J. E. Heidrich, D. C. Brown, C. I. Brady, T. A. Vander Jagt, M. Garwood, M. Bisoffi, V. Severns, D. L. Vander Jagt, L. O. Sillerud, *J. Alzheimers. Dis.* **2014**, *40*, 191.

[11] a) M. Li, P. Shi, C. Xu, J. Ren, X. Qu, *Chem. Sci.* **2013**, *4*, 2536; b) K. E. Broaders, S. Grandhe, J. M. Frechet, *J. Am. Chem. Soc.* **2011**, *133*, 756.

[12] a) S. W. Wang, Y. J. Wang, Y. J. Su, W. W. Zhou, S. G. Yang, R. Zhang, M. Zhao, Y. N. Li, Z. P. Zhang, D. W. Zhan, R. T. Liu, *Neurotoxicology* **2012**, *33*, 482; b) P. X. Xu, S. W. Wang, X. L. Yu, Y. J. Su, T. Wang, W. W. Zhou, H. Zhang, Y. J. Wang, R. T. Liu, *Behav. Brain. Res.* **2014**, *264*, 173.

[13] Y. Xiang, L. Liang, X. Wang, J. Wang, X. Zhang, Q. Zhang, *J. Controlled Release* **2011**, *152*, 402.

[14] a) Y. Ma, S. Tong, G. Bao, C. Gao, Z. F. Dai, *Biomaterials* **2013**, *34*, 7706; b) Z. J. Zhou, D. T. Huang, J. F. Bao, Q. L. Chen, G. Liu, Z. Chen, X. Y. Chen, J. H. Gao, *Adv. Mater.* **2012**, *24*, 6223; c) Y. D. Jin, C. X. Jia, S. W. Huang, M. O'Donnell, X. H. Gao, *Nat. Commun.* **2010**, *1*, 41.

[15] a) M. P. Leal, S. Rivera-Fernandez, J. M. Franco, D. Pozo, J. M. de la Fuente, M. L. Garcia-Martin, *Nanoscale* **2015**, *7*, 2050; b) Y. C. Park, J. B. Smith, T. Pham, R. D. Whitaker, C. A. Sucato, J. A. Hamilton, E. Bartolak-Suki, J. Y. Wong, *Colloid. Surface. B.* **2014**, *119*, 106; c) E. Illes, M. Szekeres, E. Kupcsik, I. Y. Toth, K. Farkas, A. Jedlovszky-Hajdu, E. Tombacz, *Colloid Surf. A* **2014**, *460*, 429.

[16] B. Wang, R. Ma, G. Liu, Y. Li, X. Liu, Y. An, L. Shi, *Langmuir* **2009**, *25*, 12522.

[17] S. C. Rogers, M. Kavdia, *Faseb. J.* **2010**, *24*, 785.

[18] J. F. Hu, S. F. Chu, N. Ning, Y. H. Yuan, W. Xue, N. H. Chen, J. T. Zhang, *Neurosci. Lett.* **2010**, *483*, 78.

[19] a) C. Corot, P. Robert, J. M. Idée, M. Port, *Adv. Drug. Delivery Rev.* **2006**, *58*, 1471; b) J. Wang, Y. Chen, B. Chen, J. Ding, G. Xia, C. Gao, J. Cheng, N. Jin, Y. Zhou, X. Li, M. Tang, X. Wang, *Int. J. Nanomed.* **2010**, *5*, 861; c) R. Weissleder, G. Elizondo, J. Wittenberg, A. S. Lee, L. Josephson, T. J. Brady, *Radiology* **1990**, *175*, 489; d) M. Taupitz, S. Wagner, J. Schnorr, I. Kravec, H. Pilgrimm, H. Bergmann-Fritsch, B. Hamm, *Invest. Radiol.* **2004**, *39*, 394.